Nodal semimetals in $d \geqslant 3$ to sharp pseudo-Landau levels by dimensional reduction

Fabian Köhler◉ and Matthias Vojta◉

*Institut für Theoretische Physik and Würzburg-Dresden Cluster of Excellence ct.qmat, Technische Universität Dresden,
01062 Dresden, Germany*

Nonuniform strain applied to graphene's honeycomb lattice can induce pseudo-Landau levels in the single-particle spectrum. Various generalizations have been put forward, including a particular family of hopping models in d space dimensions. Here we show that the key ingredient for sharp pseudo-Landau levels in higher dimensions is dimensional reduction. We consider particles moving on a d-dimensional hyperdiamond lattice which displays a semimetallic band structure, with a $(d-2)$-dimensional nodal manifold. By applying a suitable strain pattern, the single-particle spectrum evolves into a sequence of relativistic Landau levels. We develop and solve the corresponding field theory: Each nodal point effectively generates a Landau-level problem which is strictly two dimensional to leading order in the applied strain. While the effective pseudovector potential varies across the nodal manifold, the Landau-level spacing does not. Our theory paves the way for strain engineering of single-particle states via dimensional reduction and beyond global minimal coupling.

I. INTRODUCTION

Synthetic gauge fields have become an important tool to engineer phases of matter [1]: They enable one to realize phenomena associated with orbital magnetic fields for charge-neutral particles; they allow one to create non-Abelian gauge fields; and they can therefore be used to create nontrivial, often topological, states of matter. Methods to achieve synthetic gauge fields include the mechanical deformation of solid-state lattices [2–4], the rotation of atomic gases [5], laser-induced Raman transitions of cold atoms in optical lattices [6], as well as Floquet engineering in photonic crystals [7].

In solids, strain engineering is a particularly interesting route which has been used both to design novel physical phenomena and to deliver novel functionalities [2–4], the latter aspect leading to the emerging field of straintronics [8]. One particular goal is to quench the electron kinetic energy, by forming Landau levels or flat bands, such that effects of electron–electron interaction get amplified. Strain-induced pseudomagnetic fields have been first discussed for carbon nanotubes [9]. Subsequently, triaxial strain applied to graphene has been argued to induce an approximately homogeneous pseudomagnetic field for low-energy electrons, leading to relativistic pseudo-Landau levels (PLLs) [10–13]. Such PLLs have indeed been observed in strained graphene flakes [14], in graphene wafers grown on a structured substrate [15], and in artificial molecular structures [16]. Electronic PLLs induced by nonuniform strain have also been discussed for Weyl semimetals [17–20] and superconductors [21]. For insulating magnets, PLLs of Néel-state magnons [22] and of Majorana-fermion excitations of spin liquids have been proposed [23]. In all these cases, the effect of strain can be understood in terms of a pseudovector potential which influences the orbital motion of elementary excitations via minimal coupling, i.e., mimicking the effect of a physical magnetic field.

Recently, a generalization of strain-induced PLLs known for graphene to arbitrary space dimensions d has been proposed [24]. This work constructed a family of lattice models with spectral degeneracies inductively but did not provide insights into the physical mechanism leading to PLLs in higher dimensions. Other papers [25–27] proposed strain schemes for approximately flat bands in $d = 3$, but more general insights into their construction are lacking.

It is the purpose of this paper to close this gap. We consider electrons moving on the d-dimensional hyperdiamond lattice where the tight-binding dispersion is characterized by a $(d-2)$-dimensional nodal manifold. For $d = 3$ we develop and solve the continuum field theory describing the effect of tetraxial strain on the low-energy states (Fig. 1), and we generalize this theory to arbitrary $d > 3$. Remarkably, the effective theory *cannot* be understood via minimal coupling to a globally defined pseudovector potential. Instead, we show that for $d > 2$, dimensional reduction is at play: For each point on the nodal manifold a separate two-dimensional (2D) Dirac theory emerges. All of these Dirac theories generate relativistic PLLs with the *same* Landau-level spacing, and the global excitation spectrum arises from the collection of these two-dimensional Landau-level problems. We also provide a semiclassical picture for $d = 3$ which shows how dimensional reduction connects to an ensemble of anisotropic 2D electrons in a *locally* defined pseudomagnetic field. We discuss experimental realizations and generalizations.

II. HYPERDIAMOND LATTICE UNDER STRAIN

Motivated by Ref. [24], we consider particles hopping on a hyperdiamond lattice in d space dimensions: This is a bipartite lattice with coordination number $(d+1)$, leading to chain, honeycomb, and diamond lattices in $d = 1, 2, 3$, respectively. The nearest-neighbor vectors $\hat{\boldsymbol{\delta}}_j$ connect the center of a $(d+1)$ simplex to each of its vertices, these simplices
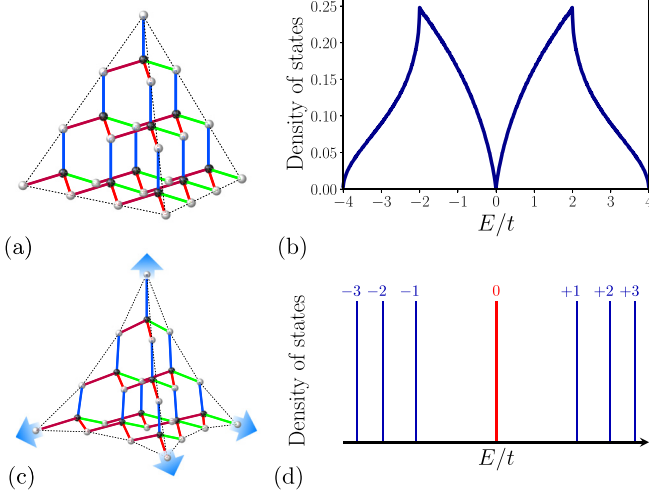
FIG. 1. Strain-induced Landau levels in $d = 3$: (a) Diamond lattice with (b) semimetallic density of states. (c) Diamond lattice under tetraxial strain, resulting in (d) sharp relativistic Landau levels which emerge via dimensional reduction.

being line segment, triangle, and tetrahedron in $d = 1, 2, 3$. In the absence of strain we have $\hat{\boldsymbol{\delta}}_j^2 = a_0^2$, $\hat{\boldsymbol{\delta}}_j \cdot \hat{\boldsymbol{\delta}}_{j'} = -a_0^2/d$ for $j \neq j'$, and $\sum_{j=1}^{d+1} \hat{\boldsymbol{\delta}}_j = \mathbf{0}$, with a_0 being the nearest-neighbor distance, which we set to unity in what follows. We consider a nearest-neighbor hopping Hamiltonian of spinless particles [28]

$$\mathcal{H} = -\sum_{\langle ii' \rangle} t_{ii'} (c_i^\dagger c_{i'} + \text{H.c.}). \tag{1}$$

In the absence of strain, $t_{ii'} \equiv t$, the momentum-space Bloch Hamiltonian takes the form $h(\boldsymbol{k}) = t\begin{pmatrix} 0 & f(\boldsymbol{k}) \\ f^*(\boldsymbol{k}) & 0 \end{pmatrix}$ in the sublattice basis, resulting in two bands with dispersion

$$\varepsilon(\boldsymbol{k}) = \pm t |f(\boldsymbol{k})|, \quad \text{where} \quad f(\boldsymbol{k}) = \sum_j \exp[-i\boldsymbol{k} \cdot \hat{\boldsymbol{\delta}}_j]. \tag{2}$$

As shown in the Supplemental Material [29], the function $f(\boldsymbol{k})$ vanishes on a $(d - 2)$-dimensional manifold in momentum space, leading to band-touching Dirac points in $d = 2$, nodal lines in $d = 3$ (Fig. 2), nodal surfaces in $d = 4$, etc. This nodal manifold is characterized by a Berry phase of π in any $d \geqslant 2$; that is, electrons encircling a nodal point along a finite-energy trajectory acquire a π phase shift.

Upon distorting the lattice, the electronic hopping amplitudes t get modified because wave-function overlaps change. Empirically, the hopping amplitudes follow [28]

$$t_{ii'} = t_0 \exp[-\beta(|\boldsymbol{R}_{ii'}|/a_0 - 1)], \tag{3}$$

where $t_0 \equiv t$ is the hopping in the absence of strain and $\boldsymbol{R}_{ii'} = \boldsymbol{r}_i + \boldsymbol{u}_i - \boldsymbol{r}_{i'} - \boldsymbol{u}_{i'}$ is the distance between sites i and i', where $\boldsymbol{u}$ is the displacement field evaluated at the lattice positions $\boldsymbol{r}_i$. The factor β encodes the strength of electron-lattice coupling: Typical values are of order unity; for graphene, $\beta = 3.37$ [30].

We subject the system to a d-dimensional generalization of the triaxial strain introduced for graphene [12]. As will become clear below, this $(d + 1)$-axial strain has the property that it generates only a pseudomagnetic field, but no pseudo-
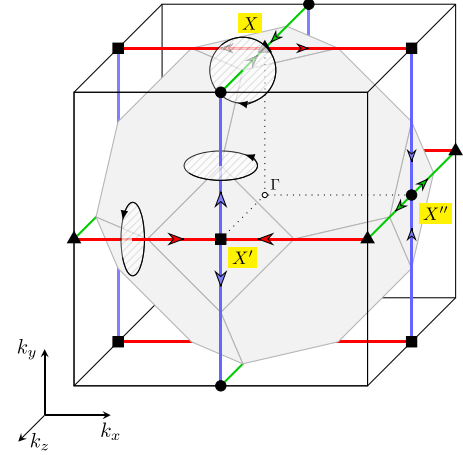

FIG. 2. Brillouin zone (shaded) of the diamond lattice, together with the momentum-space network of nodal lines which cross at the high-symmetry X points. Also shown are the directions of the pseudomagnetic field (arrows) emerging under tetraxial strain, together with the corresponding semiclassical trajectories for low-energy electrons (hatched ellipses). The pseudomagnetic field is singular at the X points.

electric field. The strain is defined by the displacement field $\boldsymbol{u}(\boldsymbol{r}) = \frac{C}{2} \sum_j (\hat{\boldsymbol{\delta}}_j \cdot \boldsymbol{r})^2 \hat{\boldsymbol{\delta}}_j$, leading to the strain tensor

$$\underline{\underline{u}} = C \sum_j (\hat{\boldsymbol{\delta}}_j \cdot \boldsymbol{r})(\hat{\boldsymbol{\delta}}_j \circ \hat{\boldsymbol{\delta}}_j). \tag{4}$$

The effect of the strain on the hopping matrix elements is now parametrized by the product $\gamma = \beta C(1 - 1/d^2)$, with the last factor included for later convenience. We note that mechanical stability limits the maximum displacement and hence the value of C, with the maximum allowed C scaling with inverse linear system size [29]. The continuum theory below relies on a Taylor expansion in C and is therefore unaware of this restriction.

III. CONTINUUM THEORY IN $d = 3$

To be specific, we demonstrate the continuum treatment for the most relevant case of $d = 3$. The tight-binding model (1) on the diamond lattice yields a dispersion featuring three distinct straight nodal lines which connect and cross at different X points [31,32]; see Fig. 2. We choose the nodal line along z and expand the Hamiltonian about an arbitrary momentum-space point on the green line segment connecting a solid circle and a solid triangle in Fig. 2, $\boldsymbol{K} = \sqrt{3}\pi/2(1, 0, \lambda)$ parametrized by $\lambda \in (0, 1)$, to obtain

$$h_{\boldsymbol{K}}(\boldsymbol{q}) = v_x(\lambda) q_x \sigma_x + v_y(\lambda) q_y \sigma_y + O(q^2), \tag{5}$$

where the full momentum is $\boldsymbol{k} = (K_x - q_x, K_y - q_y, K_z - q_z)$ and $\sigma_{x,y}$ are Pauli matrices in the sublattice space. Equation (5) is a 2D Dirac theory in the plane perpendicular to the nodal line, with velocities $v_x(\lambda) = (4t/\sqrt{3}) \cos(\frac{\pi}{2}\lambda)$, $v_y(\lambda) = (4t/\sqrt{3}) \sin(\frac{\pi}{2}\lambda)$; see Fig. 3(a). One of the velocities vanishes for $\lambda = 0, 1$, i.e., the X points where two nodal lines cross. A small-momentum expansion directly at one of the crossing
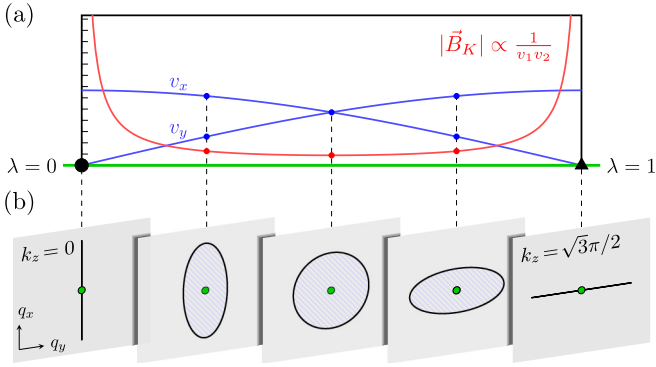
FIG. 3. Illustration of dimensional reduction in $d = 3$. (a) Dirac velocities v_x and v_y, together with the amplitude of the pseudomagnetic field $|\boldsymbol{B}_K|$, plotted along a nodal line connecting two X points. (b) Semiclassical trajectories at selected points along the nodal line in the momentum-space plane perpendicular to the nodal line.

points X yields

$$h_X(\boldsymbol{q}) = \frac{4t}{\sqrt{3}}q_x\sigma_x - \frac{4t}{3}q_yq_z\sigma_y + O(q^3); \quad (6)$$

the full momentum $\boldsymbol{k}$ here is $(\sqrt{3}\pi/2 - q_x, -q_y, -q_z)$, and we have included the quadratic piece.

We now proceed to include the effect of strain. We focus on the nodal line described by Eq. (5) and incorporate strain-induced changes of the hopping according to Eq. (3) up to first order in γ, explicitly using the $d = 3$ version of Eq. (4), i.e., tetraxial strain with $\boldsymbol{u}_{3D} = 4C/\sqrt{27}(yz, zx, xy)$; see Fig. 1. Technically, we expand about a fixed momentum-space point K on the nodal line and switch to continuum-limit real space in the plane perpendicular to this line. To leading order, this yields

$$h_K = \left(v_x(\lambda)q_x + \frac{4\gamma}{\sqrt{3}}t\sin\left(\frac{\pi}{2}\lambda\right)y\right)\sigma_x$$
$$+ \left(v_y(\lambda)q_y - \frac{4\gamma}{\sqrt{3}}t\cos\left(\frac{\pi}{2}\lambda\right)x\right)\sigma_y, \quad (7)$$

where $q_{x,y} = i\partial_{x,y}$. For fixed λ this is a Dirac theory, now minimally coupled to a pseudovector potential $\boldsymbol{A}_K = (A_x, A_y) = \frac{\gamma}{v_xv_y}(v_y^2y, -v_x^2x)$; that is, it is obtained from (5) by the replacement $\boldsymbol{q} \to \boldsymbol{q} + \boldsymbol{A}_K$. The pseudomagnetic field $\boldsymbol{B}_K$ corresponding to $\boldsymbol{A}_K$ is given by $\frac{16\gamma t^2}{3v_xv_y}(0, 0, 1)$, i.e., it is homogeneous in the $x - y$ plane, but depends on the position λ along the nodal line. These findings equivalently apply to the other nodal lines where h_K (7) then depends on the coordinates $(\bar{r}_\perp)$ and their conjugate momenta $(\bar{q}_\perp)$ perpendicular to the nodal lines, but not on the momentum $q_\parallel$ along the line. The pseudomagnetic field $\boldsymbol{B}_K$ is always directed parallel to the nodal line (Fig. 2).

IV. DIMENSIONAL REDUCTION

The form of the leading-order Hamiltonian (7) now implies that each point on a nodal line corresponds to a two-dimensional system of Dirac electrons subjected to a perpendicular homogeneous pseudomagnetic field. Since there is

no mixing between these 2D systems to this order, the total low-energy Hamiltonian can be written as

$$\mathcal{H} = \int d\boldsymbol{K}h_{\boldsymbol{K}}, \quad (8)$$

representing a sum of two-dimensional subtheories, with the integral running over the nodal manifold. While the Dirac velocities as well as the strength of the magnetic field vary along each nodal line, and moreover the field direction changes from line to line, the spectrum of pseudo-Landau levels turns out to be *independent* of λ and hence constant on the entire nodal manifold [29],

$$E_n^\pm = \pm t\sqrt{n}\sqrt{\frac{32\gamma}{3}}, \quad (9)$$

with n being the Landau-level index. Hence all nodal points generate the *same* 2D Landau-level spectrum, together resulting in sharp (i.e., nondispersive) pseudo-Landau levels with degeneracy of L^3, where L is the linear system size. Equations (8) and (9) represent the central result of this paper. Parenthetically, we note that the crossing points of two nodal lines require a separate treatment, as the pseudomagnetic field diverges, but the PLL spectrum (9) can be recovered as we will show further down.

As announced above, the spectrum (9) does not (and, in fact, cannot) emerge from the coupling of the particle motion to a globally defined pseudogauge field. Instead, electrons in each two-dimensional submanifold are subject to a different pseudogauge field $\boldsymbol{A}_K$; hence minimal coupling applies only *after* dimensional reduction.

We also note that the zeroth PLL resides on one sublattice only [24]. Similar to the case of graphene, this can be understood as a consequence of the parity anomaly of two-dimensional Dirac electrons [33].

V. SEMICLASSICAL MOTION

One can obtain a semiclassical picture of dimensional reduction by constructing a low-energy wave packet from Bloch states near a nodal momentum $\boldsymbol{K}$. Approximating the motion of the wave packet's center using Hamilton equations yields 2D orbits, parametrized by s, in the plane perpendicular to the nodal line, elliptic in both momentum space and real space [29],

$$\bar{r}_\lambda = r_0(v_x(\lambda)\cos s, -v_y(\lambda)\sin s, 0) + \text{const}, \quad (10)$$

as one would expect from a semiclassical 2D Landau problem. The orbits can be centered at an arbitrary real-space point of the 2D slice perpendicular to the nodal line, which recovers a degeneracy of L^2 per slice. Using Sommerfeld's phase-space quantization rule, together with the π Berry phase of the nodal line, yields exactly the spectrum in Eq. (9). Interestingly, this construction works for all points on the nodal lines, including their crossing points X [29].

VI. BEYOND LEADING ORDER

To access higher-order terms in both momentum and strain in the expansion of h_λ (7), it is advantageous to define the operator $\boldsymbol{\Gamma} = -i\boldsymbol{q} - \beta C_d\boldsymbol{r}$, where $C_d = C(1 - 1/d^2)$. This then

enables one to expand f in $h_K = t\begin{pmatrix} 0 & f_K \\ f_K^* & 0 \end{pmatrix}$ in powers of $\mathbf{\Gamma}$; this is facilitated by the fact that hopping and $(d + 1)$-axial strain involve terms of the form $\exp[-i\mathbf{q} \cdot \hat{\boldsymbol{\delta}}_j]$ and $\exp[-\beta C_d \mathbf{r} \cdot \hat{\boldsymbol{\delta}}_j]$, respectively, which can be combined using $\mathbf{\Gamma}$. An explicit calculation in $d = 3$ [29] yields a result which can be cast into the form

$$f_\lambda = \frac{4}{\sqrt{3}}\sqrt{2\gamma}\, a_1 + \frac{8\gamma}{3}a_\lambda a_2 + O(\Gamma^3), \qquad (11)$$

where a_1, a_2, a_λ form a complete set of commuting ladder operators, $[a_i, a_i^\dagger] = 1$, with $a_{1,2}$ (a_λ) encoding momentum and position perpendicular to (along) the nodal line, respectively.

Keeping the first-order term only restores the result above, namely a theory which is local with respect to the nodal line (in the sense that it does not involve the momentum along the nodal line) and displays the spectrum given in Eq. (9), with a degeneracy given through $a_2^\dagger a_2$. The strict dimensional reduction, however, does not hold beyond leading order due to the presence of a_λ: The physics near a chosen point K is then no longer constrained to the momentum plane perpendicular to the nodal line. Then, a rewriting of the form (8) is no longer possible, since the degrees of freedom along the nodal line would be overcounted. One may instead resort to finite patches along the nodal line and then use Eq. (11) to estimate the broadening of the PLLs; see Supplemental Material for details [29]. As the expansion (11) is controlled by powers of $\sqrt{\gamma}$, the broadening is parametrically small for small γ, i.e., small strain. Notably, the zeroth PLL remains perfectly degenerate at second order.

Taken together, beyond leading order the individual PLLs acquire a finite width, consistent with lattice calculations [24] and similar to the case of strained graphene [13,30]. The zeroth Landau level is the sharpest and hence best suited for observations and applications.

VII. GENERALIZATION TO $d > 3$

Remarkably, the above leading-order calculation can be generalized to arbitrary d, even without precise knowledge of the shape of the nodal manifold. To this end, the calculation is now performed in a coordinate-free fashion. We again expand about a nodal point K, now to first order in momentum and strain:

$$f_K = \sum_j e^{-i K \cdot \hat{\boldsymbol{\delta}}_j} \hat{\boldsymbol{\delta}}_j \cdot (\partial_r - \beta C_d r) \equiv b_K, \qquad (12)$$

where the operators ∂_r and r are defined in the plane perpendicular to the nodal manifold. As already noted above, momentum and strain terms are related by exchanging $\mathbf{q}$ and $\beta C_d \mathbf{r}$ in f_K, which allows us to introduce a bosonic operator b_K. Noting that $\omega_K = [b_K, b_K^\dagger]$ corresponds to a harmonic-oscillator energy and accounting for the 2×2 matrix structure of the Bloch Hamiltonian h_K, we find its spectrum to be $E = \pm t\sqrt{n}\sqrt{\omega_K}$. An explicit computation of ω_K shows that it is independent of K, $\omega = 2\gamma(d + 1)^2/d$ [29], such that we can define $a_1 = b_K/\sqrt{\omega}$ with $[a_1, a_1^\dagger] = 1$. Hence *all* points on the nodal manifold yield the same spectrum of pseudo-Landau

levels

$$E_n^\pm = \pm t\sqrt{n}\sqrt{2\gamma(d + 1)^2/d}, \qquad (13)$$

which is consistent with Eq. (9) for $d = 3$.

We thus conclude that $(d + 1)$-axial strain applied to the hyperdiamond lattice yields sharp PLLs with levels scaling as $\pm\sqrt{n}$ for arbitrary dimensions: The specific strain pattern guarantees that the semiclassical motion near any nodal point K is constrained to the normal space of the $(d - 2)$-dimensional Fermi manifold. Therefore the problem reduces to a family of two-dimensional Landau-level problems regardless of the dimensionality of the original model, explaining the previous lattice-model findings in Ref. [24].

VIII. CONCLUSION

We have developed and solved a continuum theory for particles hopping on a d-dimensional hyperdiamond lattice under the influence of $(d + 1)$-axial strain. This single-particle problem results in sharp PLLs in arbitrary d, which emerge for $d > 2$ via dimensional reduction: Each momentum-space point along the $(d - 2)$-dimensional nodal manifold generates an effectively two-dimensional Landau-level problem, with velocities and pseudomagnetic field varying across the manifold, but having the same (hence global) Landau-level spectrum.

Our theory opens up a non-trivial way of strain-engineering single-particle spectra: The PLLs in $d > 2$ are not generated via *global* minimal coupling, but instead arise in two-dimensional submanifolds of the system. Research on generalizations to other lattice structures is underway; a detailed investigation of the higher-dimensional valley quantum Hall effect is left for future work. Our work also raises interesting questions about interaction effects in strained hyperdiamond lattices: Will interactions also follow the principle of dimensional reduction? If yes, can one find higher-dimensional cousins of fractional quantum Hall states? If not, do novel forms of fractionalization occur for partially filled PLLs?

Our predictions can be tested in cold-atom experiments. For optical lattices, either spatial variations of beam intensities [34] or density-assisted tunneling [35] have been proposed to simulate strain effects, with the concrete goal of emulating the physics of strained graphene. The resulting PLLs can be probed using Bragg spectroscopy. We believe these settings can be generalized to $d = 3$. Alternatively, a three-dimensional generalization of the inhomogeneous photonic lattices demonstrated in Ref. [36] could be considered.

[1] M. Aidelsburger, S. Nascimbene, and N. Goldman, Artificial gauge fields in materials and engineered systems, C. R. Phys. **19**, 394 (2018).

[2] C. Si, Z. Suna, and F. Liu, Strain engineering of graphene: A review, Nanoscale **8**, 3207 (2016).

[3] B. Amorim, A. Cortijo, F. de Juan, A. G. Grushin, F. Guinea, A. Gutierrez-Rubio, H. Ochoa, V. Parente, R. Roldan, P. San-Jose, J. Schiefele, M. Sturla, and M. A. H. Vozmediano, Novel effects of strains in graphene and other two dimensional materials, Phys. Rep. **617**, 1 (2016).

[4] G. G. Naumis, S. Barraza-Lopez, M. Oliva-Leyva, and H. Terrones, Electronic and optical properties of strained graphene and other strained 2D materials: A review, Rep. Prog. Phys. **80**, 096501 (2017).

[5] A. L. Fetter, Rotating trapped Bose-Einstein condensates, Rev. Mod. Phys. **81**, 647 (2009).

[6] F. Gerbier and J. Dalibard, Gauge fields for ultracold atoms in optical superlattices, New J. Phys. **12**, 033007 (2010).

[7] M. Hafezi, Synthetic gauge fields with photons, Int. J. Mod. Phys. B **28**, 1441002 (2014).

[8] F. Miao, S.-J. Liang, and B. Cheng, Straintronics with van der Waals materials, npj Quantum Mater. **6**, 59 (2021).

[9] H. Suzuura and T. Ando, Phonons and electron-phonon scattering in carbon nanotubes, Phys. Rev. B **65**, 235412 (2002).

[10] V. M. Pereira and A. H. Castro Neto, Strain engineering of graphene's electronic structure, Phys. Rev. Lett. **103**, 046801 (2009).

[11] M. M. Fogler, F. Guinea, and M. I. Katsnelson, Pseudomagnetic fields and ballistic transport in a suspended graphene sheet, Phys. Rev. Lett. **101**, 226804 (2008).

[12] F. Guinea, M. I. Katsnelson, and A. K. Geim, Energy gaps and a zero-field quantum Hall effect in graphene by strain engineering, Nat. Phys. **6**, 30 (2010).

[13] M. Vozmediano, M. Katsnelson, and F. Guinea, Gauge fields in graphene, Phys. Rep. **496**, 109 (2010).

[14] N. Levy, S. A. Burke, K. L. Meaker, M. Panlasigui, A. Zettl, F. Guinea, A. H. Castro-Neto, and M. F. Crommie, Strain-induced pseudo-magnetic fields greater than 300 tesla in graphene nanobubbles, Science **329**, 544 (2010).

[15] P. Nigge, A. C. Qu, E. Lantagne-Hurtubise, E. Marsell, S. Link, G. Tom, M. Zonno, M. Michiardi, M. Schneider, S. Zhdanovich, G. Levy, U. Starke, C. Gutierrez, D. Bonn, S. A. Burke, M. Franz, and A. Damascelli, Room temperature strain-induced Landau levels in graphene on a wafer-scale platform, Sci. Adv. **5**, eaaw5593 (2019).

[16] K. K. Gomes, W. Mar, W. Ko, F. Guinea, and H. C. Manoharan, Designer Dirac fermions and topological phases in molecular graphene, Nature (London) **483**, 306 (2012).

[17] D. I. Pikulin, A. Chen, and M. Franz, Chiral anomaly from strain-induced gauge fields in Dirac and Weyl semimetals, Phys. Rev. X **6**, 041021 (2016).

[18] A. G. Grushin, J. W. F. Venderbos, A. Vishwanath, and R. Ilan, Inhomogeneous Weyl and Dirac semimetals: Transport in axial magnetic fields and Fermi arc surface states from pseudo-Landau levels, Phys. Rev. X **6**, 041046 (2016).

[19] A. Cortijo, D. Kharzeev, K. Landsteiner, and M. A. H. Vozmediano, Strain-induced chiral magnetic effect in Weyl semimetals, Phys. Rev. B **94**, 241405(R) (2016).

[20] R. Ilan, A. G. Grushin, and D. I. Pikulin, Pseudo-electromagnetic fields in topological semimetals, Nat. Rev. Phys. **2**, 29 (2020).

[21] G. Massarelli, G. Wachtel, J. Y. T. Wei, and A. Paramekanti, Pseudo-Landau levels of Bogoliubov quasiparticles in strained nodal superconductors, Phys. Rev. B **96**, 224516 (2017).

[22] M. M. Nayga, S. Rachel, and M. Vojta, Magnon Landau levels and emergent supersymmetry in strained antiferromagnets, Phys. Rev. Lett. **123**, 207204 (2019).

[23] S. Rachel, L. Fritz, and M. Vojta, Landau levels of Majorana fermions in a spin liquid, Phys. Rev. Lett. **116**, 167201 (2016).

[24] S. Rachel, I. Göthel, D. P. Arovas, and M. Vojta, Strain-induced Landau levels in arbitrary dimensions with an exact spectrum, Phys. Rev. Lett. **117**, 266801 (2016).

[25] E. Tang and L. Fu, Strain-induced partially flat band, helical snake states and interface superconductivity in topological crystalline insulators, Nat. Phys. **10**, 964 (2014).

[26] A. Lau, T. Hyart, C. Autieri, A. Chen, and D. I. Pikulin, Designing three-dimensional flat bands in nodal-line semimetals, Phys. Rev. X **11**, 031017 (2021).

[27] S. W. Kim and B. Uchoa, Elastic gauge fields and zero-field three-dimensional quantum Hall effect in hyperhoneycomb lattices, Phys. Rev. B **99**, 201301(R) (2019).

[28] Both the tight-binding model (1) and strain dependence of its hopping matrix elements (3) assume spatially isotropic orbitals, i.e., strictly apply to s electrons.

[29] See Supplemental Material at http://link.aps.org/supplemental/10.1103/PhysRevB.109.075123 for an analysis of the nodal manifold in arbitrary dimensions, for a detailed derivation and discussion of the continuum theory beyond leading order, and for discussions on gauge invariance and the limits to strain in the lattice models. It includes Refs. [37–46].

[30] M. Neek-Amal, L. Covaci, K. Shakouri, and F. M. Peeters, Electronic structure of a hexagonal graphene flake subjected to triaxial stress, Phys. Rev. B **88**, 115428 (2013).

[31] D. J. Chadi and M. L. Cohen, Tight-binding calculations of the valence bands of diamond and zincblende crystals, Phys. Status Solidi B **68**, 405 (1975).

[32] R. Takahashi and S. Murakami, Completely flat bands and fully localized states on surfaces of anisotropic diamond-lattice models, Phys. Rev. B **88**, 235303 (2013).

[33] H. Schomerus and N. Y. Halpern, Parity anomaly and Landau-level lasing in strained photonic honeycomb lattices, Phys. Rev. Lett. **110**, 013903 (2013).

[34] B. Tian, M. Endres, and D. Pekker, Landau levels in strained optical lattices, Phys. Rev. Lett. **115**, 236803 (2015).

[35] M. Jamotte, N. Goldman, and M. Di Liberto, Strain and pseudo-magnetic fields in optical lattices from density-assisted tunneling, Commun. Phys. **5**, 30 (2022).

[36] M. C. Rechtsman, J. M. Zeuner, A. Tünnermann, S. Nolte, M. Segev, and A. Szameit, Strain-induced pseudomagnetic field and photonic Landau levels in dielectric structures, Nat. Photon. **7**, 153 (2013).

[37] T. Kimura and T. Misumi, Lattice fermions based on higher dimensional hyperdiamond lattices, Prog. Theor. Phys. **123**, 63 (2010).

[38] C. H. Park and N. Marzari, Berry phase and pseudospin winding number in bilayer graphene, Phys. Rev. B **84**, 205440 (2011).

[39] A. H. Castro Neto, F. Guinea, N. M. R. Peres, K. S. Novoselov, and A. K. Geim, The electronic properties of graphene, Rev. Mod. Phys. **81**, 109 (2009).

[40] M. Ramezani Masir, D. Moldovan, and F. M. Peeters, Pseudo magnetic field in strained graphene: Revisited, Solid State Commun. **175-176**, 76 (2013).

[41] A. L. Kitt, V. M. Pereira, A. K. Swan, and B. B. Goldberg, Lattice-corrected strain-induced vector potentials in graphene, Phys. Rev. B **85**, 115432 (2012); **87**, 159909(E) (2013).

[42] C. Tőke, P. E. Lammert, V. H. Crespi, and J. K. Jain, Fractional quantum Hall effect in graphene, Phys. Rev. B **74**, 235417 (2006).

[43] D. Xiao, M.-C. Chang, and Q. Niu, Berry phase effects on electronic properties, Rev. Mod. Phys. **82**, 1959 (2010).

[44] J. N. Fuchs, F. Piechon, M. O. Goerbig, and G. Montambaux, Topological Berry phase and semiclassical quantization of cyclotron orbits for two-dimensional electrons in coupled band models, Eur. Phys. J. B **77**, 351 (2010).

[45] J. L. Mañes, F. de Juan, M. Sturla, and M. A. H. Vozmediano, Generalized effective Hamiltonian for graphene under non-uniform strain, Phys. Rev. B **88**, 155405 (2013).

[46] E. V. Castro, M. A. Cazalilla, and M. A. H. Vozmediano, Raise and collapse of pseudo Landau levels in graphene, Phys. Rev. B **96**, 241405(R) (2017).